1 **TITLE:**

2 ***In vivo* KRAS G12D/V degradation mediated by CANDDY using a modified**

3 **proteasome inhibitor**

4

5 **AUTHORS/AFFILIATIONS:**

6 **Satoshi Imanishi[1,#], Lijuan Huang[1,#], Shoko Itakura[2], Masamichi Ishizaka[1], Yoichi**

7 **Iwasaki[1], Tomohiro Yamaguchi[1], and Etsuko Miyamoto-Sato[1,2*]**

8 [1] Laboratory of Miyamoto-Sato Molecular Medical Sciences, Research Institute for

9 Science & Technology, Tokyo University of Science, 2641 Yamazaki, Noda, Chiba

10 278-0022, Japan

11 [2]Graduate School of Biological Sciences, Tokyo University of Science, 2641 Yamazaki,

12 Noda, Chiba 278-0022, Japan

13

14 [#]These authors contributed equally to this work.

15 [*] Correspondence: nekoneko@rs.tus.ac.jp

16

Abstract

"Undruggable" proteins, such as RAS proteins, remain problematic despite efforts to discover inhibitors against them. KRAS mutants are prevalent in human cancers. Recently, the KRAS G12C inhibitor have been clinically approved, but inhibitors for KRAS G12D/V are still under development. Here, we described the development of a novel chemical knockdown strategy, termed CANDDY (Chemical knockdown with Affinity aNd Degradation DYnamics). This strategy involves a CANDDY tag modified from a proteasome inhibitor inducing direct proteasomal degradation. We constructed TUS-007 as a multispecific small molecule tethered from a KRAS interactor and CANDDY tag to target KRAS G12D/V. We confirmed that the degradation by TUS-007 was independent of target ubiquitination. This allows to solve a laborious design of matchmaker in the current ubiquitination-dependent proteolysis technology. And TUS-007 successfully suppressed tumors due to *in vivo* degradation of KRAS G12D/V. The CANDDY technology could represent a simple and rational strategy to degrade currently "undruggable" proteins.

32 **Main Text**

33 The majority (75%) of disease-causing proteins are "undruggable" (i.e., difficult to
34 inhibit with small molecules). This difficulty reflects in the presence of smooth surfaces
35 and lack of deep pockets, including proteins associated with cancer drivers and many
36 interfaces for protein-protein interaction (PPI) (1, 2, 3). RAS family members (e.g.,
37 KRAS, HRAS, and NRAS) are most challenging to inhibit by small molecules (1, 4, 5,
38 6, 7). Mutations of KRAS, especially G12C, G12D, and G12V, are frequent in human
39 cancers (7). The RAS protein activities depend on nucleotide loading in their GTP-
40 binding pockets. The inhibition of this pocket has been attempted for nearly 40 years.
41 However, progress has been hindered by the exceptionally high affinity between GTP
42 and RAS proteins (1, 4, 8). While the inhibitor targeting KRAS G12C have been
43 clinically approved recently (6, 9), inhibitors for KRAS G12D/V, which addresses
44 greater clinical need, are still remained under development. These are important targets
45 found in 95% of pancreatic cancers and 64% of colon cancers (7, 8). Inhibitors of the
46 PPI between RAS and Son of Sevenless 1 (SOS1) (RAS-SOS inhibitor) have been
47 investigated. Inhibitors that directly bind to RAS are not effective owing to their low

48 affinity (5). Thus, the current inhibition technologies are not enough to be effective for
49 undruggable proteins.
50 Pharmaceutical research on undruggable proteins, such as RAS, focuses on novel
51 modalities instead of inhibition (10, 11, 12). Proteolysis technologies, using
52 matchmakers between the target and E3 ligase or other ubiquitination related proteins
53 such as molecular chaperons for inducing target degradations, are expected to be
54 effective against undruggable proteins (13, 14, 15, 16, 17). However, matchmaker
55 design has been hampered by the dependency on target ubiquitination (16). It is difficult
56 to select a suitable E3 ligase for a target of interest because of limited knowledge about
57 the mechanism underlying substrate recognition by E3 ligases. Even if the target has an
58 established corresponding E3 ligase, there may be no available ligand for the E3 ligase.
59 Moreover, target ubiquitination may not always induce proteolysis, as in the case of
60 RAS, in which ubiquitination also regulates protein localization and activation (18).
61 Despite such difficulties, an effective inhibitor (9) was used recently for a proteolysis
62 inducer of KRAS G12C (19). However, no proteolysis inducer for KRAS G12D/V has
63 been reported. Current proteolysis technologies that depend on ubiquitination have

64 limited efficacy for undruggable targets (14). Therefore, to modulate diverse

65 undruggable targets, the difficulties in matchmaking should be eliminated (13).

66 Here, we report successful KRAS G12D/V degradation, mediated by a novel tool

67 named CANDDY (Chemical knockdown with Affinity aNd Degradation DYnamics).

68 This innovative approach induces direct proteasomal degradation (i.e., chemical

69 knockdown) of the target using a CANDDY tag derived from a proteasome inhibitor

70 that lacks the site for inhibitory activity (inhibitor site). By CANDDY technology,

71 chemical knockdown occurs without ubiquitination, so it can bypass the difficulties of

72 designing a matchmaker in current proteolysis techniques (13). Using an inefficient

73 target inhibitor, RAS/SOS inhibitor (5), we designed and synthesized a CANDDY

74 molecule called TUS-007 for KRAS G12D/V. We demonstrated KRAS G12D/V

75 chemical knockdown mediated by TUS-007 in cell-free, *in vitro*, and *in vivo* assays,

76 and *in vivo* tumor suppression.

77

78 **Results**

79 **A CANDDY molecule for targeting KRAS G12D/V proteins**

80 CANDDY molecules are bispecific molecules constructed from two modules;

81 a target interactor, which enables specific binding to the target, and a CANDDY tag,

82 which induces proteasomal degradation (Fig. 1a). The CANDDY tag is essential in

83 CANDDY technology and is a derivative lacking the inhibitor site of MLN2238 (MLN)

84 (20), a clinical proteasome inhibitor (Fig. 1b and Supplementary Information). To

85 design TUS-007, we employed a RAS-SOS inhibitor (5) (shown in Fig. 1c) which

86 directly binds to KRAS G12D, KRAS G12V, and wild-types of KRAS and HRAS as

87 the target interactor module. Since the binding to wild-type NRAS have not been

88 reported, it was expected to avoid the severe toxicity observed in a pan-RAS inhibitor

89 (21). RAS-SOS inhibitor was conjugated to the CANDDY tag using a NH_2 linker (Fig.

90 1c and Supplementary Information).

91 To compare the target binding of TUS-007 with that of the RAS-SOS

92 inhibitor, we performed a thermal shift assay. Unexpectedly, KRAS G12D/V proteins

93 incubated with TUS-007 were more resistant against heat treatment than those

94 incubated with RAS-SOS inhibitor (Fig. 1d). Alternatively, in a fluorescence-based

95 thermal shift assay, the T_m value of KRAS G12D incubated with TUS-007 was higher

96 than that of KRAS G12D incubated with RAS-SOS inhibitor (Supplementary Fig. 1).

97 These results suggest the higher affinity of TUS-007 to KRAS compared to RAS-SOS

98 inhibitor. In addition, we confirmed that TUS-007 had no inhibitory activity against the

99 catalytic β-subunits of proteasome (Supplementary Fig. 2). This demonstrated that the

100 CANDDY tag, modified from a proteasome inhibitor, hardly inhibit proteasome

101 activity.

102

103 **Chemical knockdown of KRAS G12D/V free from ubiquitination by TUS-007**

104 We attempted a chemical knockdown of KRAS G12D in the presence of 26S

105 proteasomes and in the absence of any ubiquitination related proteins in a cell-free

106 assay. Successful degradation was performed with 50% degradation concentration

107 (DC50) at 4 μM (Supplementary Fig. 3a). The chemical knockdown mediated by TUS-

108 007 was counteracted by the presence of MLN (Fig. 1e). Additionally, RAS-SOS-NH_2

109 (a synthetic intermediate without CANDDY tag, Fig. 1c) as a degradation-incompetent

110 control failed to induce the chemical knockdown (Fig. 1e), demonstrating CANDDY

111 tag is essential to induce the chemical knockdown. Although RAS-SOS inhibitor

112 showed 80% inhibition of RAS-SOS PPI at 1 mM (5), DC80 of TUS-007 for KRAS

113 G12D was estimated as 16 μM (Supplementary Fig. 3a). It implied that the conjugation

114 with CANDDY tag drastically improved the usefulness of RAS-SOS inhibitor. We also

115 confirmed chemical knockdown of KRAS G12V by TUS-007 in a cell-free assay in the

116 absence of any ubiquitination related proteins (Supplementary Fig. 3b). Furthermore, to

117 obtain additional evidence of degradation independent of ubiquitination, we co-treated

118 HeLa cells expressing GFP-KRAS G12D and DsRed with TUS-007 and MLN, E1

119 inhibitor (NAEi) or HSP70 inhibitor (VER-155008) (Supplementary Fig. 4). MLN

120 counteracted the lowering of GFP signal induced by TUS-007 treatment, but NAEi or

121 VER-155008 did not. These results demonstrated that chemical knockdown induced by

122 TUS-007 was depend on proteasome and independent of ubiquitination processes.

123

124 **TUS-007 induced targets-selective chemical knockdown *in vitro***

125 Using an *in vitro* assay, we then evaluated the chemical knockdown and

126 investigated the selectivity of TUS-007. We utilized RAS-less mouse embryonic

127 fibroblasts (MEFs) expressing human KRAS G12D, G12V, or G12C. These MEFs do

128 not proliferate in the absence of RAS (22). Immunoblotting analysis revealed that TUS-
129 007 induced the chemical knockdown of KRAS G12D/V, but not G12C, in RAS-less
130 MEFs (Fig. 1f). TUS-007 reduced the viability of RAS-less MEFs expressing KRAS
131 G12D/V but did not affect the viability of the cells expressing KRAS G12C (Fig. 1g),
132 confirming the selectivity of TUS-007 for KRAS G12D/V. We also assessed the
133 selectivity of TUS-007 for the human RAS family, including wild-type KRAS, HRAS,
134 and NRAS. TUS-007 did not affect the NRAS protein levels or the viability of RAS-
135 less MEFs expressing NRAS but affected KRAS or HRAS levels and the viability of
136 RAS-less MEFs expressing KRAS or HRAS (Supplementary Fig. 5a and b). This result
137 is consistent with the previously reported data on the selectivity of the RAS-SOS
138 inhibitor (5). Therefore, it is expected not to induce intolerable toxicity previously
139 observed with a pan-RAS inhibitor *in vivo* (21) since TUS-007 is not a pan-RAS
140 degrader. Furthermore, the viability of RAS-less MEFs expressing KRAS G12C
141 maintained even at 100 μM TUS-007 (Fig. 1f and g), indicating that TUS-007 might
142 have no remarkable off-target toxicity in cell even at high concentrations. These results

143 demonstrated the correlation between the degradation of targets and the viability of cells

144 by the concentrations of TUS-007 without non-specific cytotoxic effect (Fig. 1f and g).

145

146 **The effects of TUS-007 on KRAS G12V-driven colon cancer**

147 Approximately 64% of human colon cancers reportedly express KRAS

148 mutants. KRAS G12V is found in nearly half of the patients and is correlated with poor

149 prognosis (8). Therefore, we investigated whether TUS-007 can suppress the growth of

150 human KRAS G12V-driven colon cancer cells. We conducted an experiment with the

151 SW620-Luc KRAS G12V homozygous human colon cancer cell line (23). TUS-007

152 induced chemical knockdown of KRAS (Fig. 2a), accompanied by an increase in the

153 annexin V-positive fraction in SW620-Luc cells (Fig. 2b and Supplementary Fig. 6).

154 However, RAS-SOS-NH_2 and cetuximab did not induce apoptosis (Fig. 2b and

155 Supplementary Fig. 6). In contrast, treatment with TUS-007 did not result in significant

156 changes in the annexin V-positive fraction in HT29-Luc RAS-independent colon cancer

157 cells (Fig. 2c and Supplementary Fig. 7). Alternatively, the apoptosis induction in

158 SW620-Luc cells was confirmed by caspase 3/7 activation (Fig. 2d). Importantly, TUS-

159 007 induced the apoptosis in SW620-Luc cells at the same concentration at which the

160 chemical knockdown of KRAS was significant (Fig. 2a, b and Supplementary Fig. 8).

161 These findings indicated that TUS-007 selectively induces apoptosis in SW620-Luc

162 cells by chemical knockdown of KRAS G12V *in vitro*.

163 Next, to assess the effectiveness of TUS-007 *in vivo*, we transplanted SW620-

164 Luc cells subcutaneously in immunodeficient mice. TUS-007 or cetuximab was

165 administered to the xenograft mice by intraperitoneal (i.p.) injection. TUS-007

166 significantly attenuated tumor progression (Fig. 2e, f and Supplementary Fig. 9a) and

167 induced KRAS G12V chemical knockdown in tumors (Supplementary Fig. 9b). The

168 body weights of the mice were not affected by TUS-007 treatment (Supplementary Fig.

169 9c). These results suggested that TUS-007 is effective *in vivo* against KRAS G12V-

170 driven tumors.

171

172 **The effects of TUS-007 on KRAS G12D-driven pancreatic cancer**

173 Approximately 95% of pancreatic cancers harbor KRAS mutations, and the

174 G12D mutation is particularly prevalent and strongly correlated with poor prognosis (8).

175 Therefore, we examined the effects of TUS-007 in human pancreatic cancer cell lines.

176 As expected, TUS-007 degraded the KRAS protein (Fig. 3a) and induced apoptosis

177 (Fig. 3b) in SW1990 KRAS G12D-driven pancreatic cancer cells (24). The apoptosis

178 induction in SW1990 cells was approximately correlated with concentrations of

179 chemical knockdown of KRAS (Fig. 3a and b). The correlation between the

180 concentration of apoptosis induction and degradation induction was further confirmed

181 (Supplementary Fig. 10). In addition, apoptosis was induced with caspase 3/7 activation

182 in SW1990 cells (Fig. 3c), which was counteracted by a proteasome inhibitor MLN but

183 not by a ubiquitination inhibitor NAEi (Fig. 3d). Therefore, it suggested that TUS-007

184 induced apoptosis owing to target degradation independent of ubiquitination.

185 In mice with SW1990 cells implanted subcutaneously, the oral (per os; p.o.)

186 administration of TUS-007 significantly suppressed the tumor growth (Fig. 3e) and

187 reduced tumor weight (Supplementary Fig. 11a). The i.p. injection of TUS-007 also

188 suppressed subcutaneously implanted tumor growth in mice (Supplementary Fig. 11b).

189 Both p.o. (Fig. 3f) and i.p. (Supplementary Fig. 11c) administrations showed no change

190 in body weight. Here, we examined the chemical knockdown of KRAS, HRAS and

191 NRAS with TUS-007 in pancreas from the identical mice used in Fig. 3e and f. In

192 accordant with the results in RAS-less MEFs, TUS-007 induced the degradation of

193 KRAS and HRAS but not NRAS (Supplementary Fig 12). Thus, there was no sign of

194 toxicity such as body weight losses in contrast to a pan-RAS inhibitor (21).

195 Moreover, extracellular signal-regulate kinase (ERK) and protein kinase B

196 (AKT) phosphorylation were decreased in tumor by both p.o. and i.p. administrations

197 (Supplementary Fig. 13a and b), indicating that both RAS-mitogen-activation protein

198 (RAS-MAP) and RAS- phosphoinositide 3-kinase (RAS-PI3K) signaling were

199 inhibited. It is difficult for inhibitors to inhibit both RAS-MAP and RAS-PI3K

200 signaling, even using a clinically effective KRAS G12C inhibitor (6). Thus, the

201 chemical knockdown of KRAS by CANDDY might offer a clinical benefit. Taken

202 together, these results indicated that TUS-007 exerted *in vivo* antitumor activity *via* the

203 chemical knockdown of KRAS G12D/V and suppression of KRAS signaling.

204

205 **TUS-007 exerted anti-tumor activity even in orthotopic xenograft model mice**

206 SW1990-Luc cells were transplanted directly into the pancreas of mice as an
207 orthotopic xenograft model. The mice were subsequently treated p.o. with TUS-007.
208 Remarkably, *in vivo* imaging revealed reductions in tumor growth (Fig. 4a, b and
209 Supplementary Fig. 14a) and tumor weight (Supplementary Fig. 14b). Results from
210 immunohistochemical analysis (Fig. 4c left panels and Supplementary Fig. 14c left bar
211 graph) and immunoblotting (Fig. 4d) confirmed the chemical knockdown of KRAS
212 G12D in the tumor tissues of mice treated with TUS-007. Furthermore, higher
213 concentrations of positive cells were observed in the terminal deoxynucleotidyl
214 transferase dUTP nick-end labeling (TUNEL) assay in the tumor tissues of TUS-007-
215 treated mice, implying the induction of apoptosis in the TUS-007-treated tumors (Fig.
216 4c right panels and Supplementary Fig. 14c right bar graph). The body weights of the
217 orthotopic xenograft model mice were not affected by TUS-007 (Supplementary Fig.
218 14d). Overall, these results demonstrated that oral treatment with TUS-007 induces
219 KRAS G12D chemical knockdown and suppresses pancreatic tumor growth without the
220 sign of weight loss and significant toxicity in the orthotopic xenograft model.

221 Finally, we examined the *in vivo* concentrations of TUS-007. When an i.p

222 dose of 80 mg/kg TUS-007 was administered to healthy mice, a concentration (45

223 ng/mg, equivalent to 53 μM) of TUS-007 was observed in the pancreas (Supplementary

224 Table 1.). This TUS-007 concentration *in vivo* agreed with the concentration at which

225 chemical knockdown and apoptotic indicators were observed in SW1990 cells *in vitro*

226 (Fig. 3a-c). Therefore, these results suggest that there is no contradiction between our *in*

227 *vivo* and *in vitro* results.

228

229 **CANDDY applied to another undruggable target**

230 To evaluate the versatility of CANDDY approach, we designed a CANDDY

231 molecule targeting MDM2 (MDM2-CANDDY), a negative regulator of P53, using a

232 P53-MDM2 PPI inhibitor with a weak potency (25) as an interactor module of a

233 CANDDY molecule (Supplementary Fig. 15a and Supplementary Information).

234 MDM2-CANDDY successfully induced the chemical knockdown of MDM2 in HCT-

235 116 human colon cancer cells (Supplementary Fig. 15b). P53-MDM2 PPI is still well-

236 recognized “undruggable” target (26). This result suggested the potential versatility of

237 CANDDY to target other undruggable proteins.

238

239 **Discussion**

240 We provided the proof of concept that CANDDY tag enabled to induce

241 proteasomal degradation through ubiquitination-independent process (Fig. 1e and

242 Supplementary Fig. 4) in this report. Considering the proteasome enable to degrade any

243 targets, the CANDDY tag modified from a proteasome inhibitor (Fig. 1b) can eliminate

244 the difficulties of matchmaking of targets and specific ubiquitination related proteins

245 such as E3 ligases in current protein degradation (13, 14). Thus, CANDDY technology

246 could provide a simple and rational approach to induce the chemical knockdown of

247 currently undruggable targets because of the CANDDY tag independent of

248 ubiquitination.

249 Expectedly, we confirmed the correlations between degradation of KRAS

250 G12D and V and apoptosis in pancreatic and colon cancer cells, respectively (Fig. 2a, b,

251 Fig. 3a-d, Supplementary Fig. 8 and 10), and *in vivo* (Fig. 4c and Supplementary Fig.

252 14c). Both *in vitro* and *in vivo*, TUS-007 achieved efficacy mediated by moderate

253 degradations of KRAS G12D/V. A previous study showed that the moderate decrease of

254 KRAS protein is enough to inhibit tumor growth *via* more strong inhibition of

255 downstream signal (12) as well as we showed (Supplementary Fig. 13). Thus, *in vitro*

256 and *in vivo* results could be reasonable. Importantly, the concentration of TUS-007 in

257 pancreas agreed with the effective concentration *in vitro* (Supplementary Table1),

258 demonstrating the consistency between our *in vivo* and *in vitro* results. On the other

259 hand, the requirement of high concentrations generally raises concerns about toxicity.

260 However, TUS-007 did not show non-specific cytotoxicity *in vitro* even at high

261 concentration (Fig. 1g) and no sign of body weight losses was observed in TUS-007

262 treated mice (Fig. 3f, Supplementary Fig. 9c, 11c and 14d) in contrast to a pan-RAS

263 inhibitor (21). These results suggest that TUS-007 induced *in vivo* degradation of

264 KRAS G12D/V resulting in suppression of colon and pancreatic tumors without no

265 significant toxicity even at high concentrations.

266 No effective drug to inhibit or degrade KRAS G12D/V has been reported yet.

267 Also, the proteolysis field does not still have enough evidence that can target and

268 degrade tough and valuable undruggable proteins (14). Of note, in spite of a poor

269 inhibitor was employed as interactor, TUS-007 induced chemical knockdown of KRAS

270 G12D/V *in vivo*, resulting in suppression of a pancreatic tumor even in the orthotopic

271 xenograft model with oral administrations (Fig. 4). In addition, another weak inhibitor

272 of PPI, P53-MDM2 PPI inhibitor (25) (Supplementary Fig. 15), was useful as the

273 interactor of CANDDY molecules. Thus, CANDDY technology could be expectedly

274 applied to tough and valuable undruggable targets still remaining with no effective

275 inhibitors. In the future, CANDDY has the potential to overcome the current limitations

276 of proteolysis and to expand the application scope of degraders for molecular targeting

277 therapy of aggressive and deadly diseases caused by undruggable targets.

278

References

1. Khan, I., Rhett, J. M. & O'Bryan, J. P. Therapeutic targeting of RAS: New Hope for drugging the "undruggable". *Biochim. Biophys. Acta Mol. Cell Res.* **1867**, 118570 (2020).
2. Fujimori, S., et al. Next-generation sequencing coupled with a cell-free display technology for high-throughput production of reliable interactome data. *Sci. Rep.* **2,** 691 (2012).
3. Scott, D. E., Bayly, A. R., Abell, C. & Skidmore, J. Small molecules, big targets: Drug discovery faces the protein-protein interaction challenge. *Nat. Rev. Drug Discov.* **15,** 533–550 (2016).
4. Stephen, A. G., Esposito, D., Bagni, R. K. & McCormick, F. Dragging Ras back in the ring. *Cancer Cell* **25,** 272–281 (2014).
5. Sun, Q., et al. Discovery of small molecules that bind to K-Ras and inhibit Sos-mediated activation. *Angew. Chem. Int. Ed.* **51,** 6140–6143 (2012).
6. Canon, J., et al. The clinical KRAS(G12C) inhibitor AMG 510 drives anti-tumour immunity. *Nature* **575,** 217–223 (2019).

296 7. Hobbs, G. A., Der, C. J. & Rossman, K. L. RAS isoforms and mutations in cancer at
297 a glance. *J. Cell Sci.* **129,** 1287–1292 (2016).
298 8. Haigis, K. M. KRAS alleles: The devil is in the detail. *Trends Cancer* **3,** 686–697
299 (2017).
300 9. Sheridan, C. Grail of RAS cancer drugs within reach. *Nat. Biotechnol.* **38,** 6–8
301 (2020).
302 10. Shin, S. M., et al. Antibody targeting intracellular oncogenic Ras mutants exerts
303 anti-tumour effects after systemic administration. *Nat. Commun.* **8,** 15090 (2017).
304 11. Yin, W. & Rogge, M. Targeting RNA: A transformative therapeutic strategy. *Clin.*
305 *Transl. Sci.* **12,** 98–112 (2019).
306 12. Ross, S. J., et al. Targeting KRAS-dependent tumors with AZD4785, a high-affinity
307 therapeutic antisense oligonucleotide inhibitor of KRAS. *Sci. Transl. Med.* **9,** pii:
308 eaal5253. doi: 10.1126/scitranslmed.aal5253 (2017).
309 13. Deshaies, R. J. Multispecific drugs herald a new era of biopharmaceutical
310 innovation. *Nature* **580,** 329–338 (2020).

311 14. Scudellari, M. Protein-slaying drugs could be the next blockbuster therapies. *Nature*
312 **567,** 298–300 (2019).
313 15. Cromm, P. M. & Crews, C. M. Targeted protein degradation: From chemical
314 biology to drug discovery. *Cell Chem. Biol.* **24,** 1181–1190 (2017).
315 16. Pettersson, M. & Crews, C. M. PROteolysis TArgeting Chimeras (PROTACs) -
316 Past, present and future. *Drug Discov. Today Technol.* **31,** 15–27 (2019).
317 17. Churcher, I. Protac-induced protein degradation in drug discovery: Breaking the
318 rules or just making new ones? *J. Med. Chem.* **61,** 444–452 (2018).
319 18. Dohlman, H. G. & Campbell, S. L. Regulation of large and small G proteins by
320 ubiquitination. *J. Biol. Chem.* **294,** 18613–18623 (2019).
321 19. Bond, M. J., et al. Targeted degradation of oncogenic KRASG12C by VHL-
322 recruiting PROTACs. *ACS Cent. Sci.* **6**, 1367–1375 (2020).
323 20. Kisselev, A. F., van der Linden, W. A. & Overkleeft, H. S. Proteasome inhibitors:
324 An expanding army attacking a unique target. *Chem. Biol.* **19,** 99–115 (2012).
325 21. Welsch, M. E., et al. Multivalent small-molecule pan-RAS inhibitors. *Cell* **168,**
326 878–889.e29 (2017).

327 22. Drosten, M., et al. Genetic analysis of Ras signaling pathways in cell proliferation,
328 migration and survival. *EMBO J.* **29,** 1091–1104 (2010).
329 23. Ahmed, D., et al. Epigenetic and genetic features of 24 colon cancer cell lines.
330 *Oncogenesis* **2,** e71 (2013).
331 24. Jansen, J. M., et al. Inhibition of prenylated KRAS in a lipid environment. *PLOS*
332 *ONE* **12,** e0174706 (2017).
333 25. Kumar, S. K., et al. Design, synthesis, and evaluation of novel boronic-Chalcone
334 derivatives as antitumor agents. *J. Med. Chem.* **46**, 2813–2815 (2003).
335 26. Shangary, S. & Wang, S. Targeting the MDM2-p53 Interaction for Cancer Therapy.
336 *Clin. Cancer. Res.* **14,** 5318–5324 (2008).
337 27. Scott, D. E., Bin, Y. & Charlene F. Proteolysis targeting chimeras (PROTACs) in
338 'beyond rule-of-five' chemical space: Recent progress and future challenges, *Bioorg*
339 *Med Chem Lett*, **29**, 1555–1564 (2019).
340

341 **Data availability**

342 Source data are provided for all experiments. Other data that support the

343 findings of this study are available from the corresponding author, upon reasonable

344 request.

345

346 **Acknowledgments** We thank Masaaki Ozawa, Mai Hasegawa, Takuya Yogi, Mizuki

347 Kanazawa, and Sachi Tsuji for help with the *in vitro* studies, Yuri Sato for help with the

348 *in vivo* studies, Megumi Tsukamoto and Megumi Saito for help with both *in vitro* and *in*

349 *vivo* studies. We thank the NCI RAS initiative for providing the RAS-less MEFs used

350 in this work, the Uchiro Laboratory for performing the high-resolution mass

351 spectrometry analysis at the Research Equipment Center (Tokyo University of Science

352 (TUS), Japan), the Gunji Laboratory (TUS) for the use of their high-performance liquid

353 chromatography instruments, the Iwakura and Abe Laboratories in the animal facility of

354 the Research Institute for Biomedical Sciences (TUS) for maintaining the mice, Fumito

355 Ishizuka and Naoki Takeda (NARD Institute, Ltd.) for contributions to the chemical

356 synthesis, and Hiroyuki Ohashi for the helpful suggestions. This work was financially

supported by the Program for Creating STart-ups from Advanced Research and Technology (START Program: 962238), and the joint research with FuturedMe Inc.

Author contributions S. Im., L. H., S. It., and E. M. S. designed the study. S. Im., L. H., S. It., M. I. and T. Y. performed the *in vitro* and *in vivo* experiments. Y. I. performed chemical analyses. E. M. S. supervised the study. All authors discussed the study and approved the submitted manuscript.

Competing interests The authors declare no competing interests.

Supplementary Information is available in the online version of the paper.

370 **Figure legends**

371

372 **Fig. 1. RAS chemical knockdown *in vitro*.**

373 **a,** Principle of the CANDDY technology. Each CANDDY molecule includes a target

374 interactor (burgundy hexagon) and a CANDDY tag (yellow oval). The target protein is

375 bound by the CANDDY molecule *via* the target interactor and is directly degraded by

376 proteasome via the CANDDY tag. **b,** The CANDDY tag was synthesized by chemically

377 inactivating the inhibitor site of MLM2238 (MLN). **c,** Structures of the RAS-SOS

378 inhibitor (ref. 5), RAS-SOS-NH_2, and TUS-007. **d,** Evaluation of the target-binding

379 affinity of TUS-007 to KRAS mutants by a thermal shift assay. Recombinant KRAS

380 was treated with the vehicle, RAS-SOS inhibitor, or TUS-007 for 30 min, heated at the

381 indicated temperature for 20 min, then analyzed by immunoblotting. **e,** TUS-007

382 induced KRAS G12D chemical knockdown by 26S proteasome in a cell free assay.

383 KRAS G12D incubated with 26S proteasome and agents as indicated for 3 h. **f & g,**

384 RAS-less MEFs expressing KRAS G12D, G12V or G12C were incubated with TUS-

385 007 for 72 h. Representative blots of KRAS are shown (**f**). The relative amounts of

386 KRAS mutants normalized to GAPDH are shown in the bar graph (mean ± SEM; n = 3–

387 4). The cell viability was also measured (mean ± SEM; n = 3–4) (**g**). *P < 0.05 and **P

388 < 0.01 vs. DMSO.

389

390 **Fig. 2. Chemical knockdown and tumor suppression *in vitro* and *in vivo* in KRAS**

391 **G12V-driven human colon cancer cells by TUS-007 treatment.**

392 **a,** Immunoblotting analysis of KRAS G12V chemical knockdown in SW620-Luc cells

393 treated with TUS-007 for 48 h at the indicated doses. The KRAS band intensity was

394 normalized to that of GAPDH (mean ± SEM; n = 3). *P < 0.05 and **P < 0.01 vs.

395 DMSO. **b & c,** The ratio of apoptotic cells were analyzed in colon cancer SW620-Luc

396 cells (**b**) and HT29-Luc cells (**c**), a KRAS-independent, BRAF-dependent cell line (Ctx

397 + Vem: 100 mg/ml cetuximab and 40 mM vemurafenib). Cells were treated with each

398 compound for 48 h in terms of the number of annexin V-positive/PI-negative apoptotic

399 cells detected by flow cytometry (mean ± SEM; n = 2–5). **P < 0.01, and ***P < 0.001

400 vs. DMSO. **d,** Relative activity of caspase 3/7 in SW620-Luc cells treated with TUS-

401 007 or 5-fluorouracil (5-FU) for 48 h (mean ± SEM; n = 3). *P < 0.05 and **P < 0.01

402 vs. DMSO. **e,** Tumor volume in mice with SW620-Luc cells transplanted

403 subcutaneously and treated with i.p. administration every 3 days (mean ± SEM; n = 6–

404 8). *P < 0.05 vs. vehicle alone. **f,** Tumors of SW620-Luc cells at day 21 from the same

405 mice shown in **e** (n = 6–8).

406

407 **Fig. 3. Chemical knockdown and tumor suppression *in vitro* and *in vivo* in KRAS**

408 **G12D-driven human pancreatic cancer cells by TUS-007 treatment.**

409 **a,** KRAS G12D chemical knockdown induced by TUS-007 in SW1990 cells. SW1990

410 cells were treated with TUS-007 for 72 h and analyzed by immunoblotting. The KRAS

411 G12D band intensity was normalized to that of GAPDH (mean ± SEM; n = 4). *P <

412 0.05 vs. DMSO. **b,** The proportion of annexin V-positive apoptotic SW1990 cells

413 treated with DMSO, RAS-SOS-NH_2 or TUS-007 for 72 h (mean ± SEM; n = 3). *P <

414 0.05 vs. DMSO or RAS-SOS-NH_2. **c,** TUS-007 increased the caspase 3/7 activity in

415 SW1990 cells after treatment for 96 h (mean ± SEM; n = 3). *P < 0.05 and **P < 0.01

416 vs. DMSO. **d,** Caspase 3/7 activation by TUS-007 was proteasome dependent and

417 ubiquitination independent. SW1990 cells were treated with the agents for 96 h (mean ±

418 SEM; n = 3). **P < 0.01 vs. DMSO, ##P < 0.01 vs. TUS-007 (100 μM) only, and †no

419 statistically significant difference compared with TUS-007 (100 μM) only. **e,** Tumor

420 volume in mice with SW1990 cells transplanted subcutaneously and treated with p.o.

421 administered TUS-007 or vehicle (mean ± SEM; n = 6–9). The agents were

422 administered every 3 days. **P < 0.01 vs. vehicle alone. **f,** Body weight changes in

423 mice with SW1990 cells transplanted subcutaneously (mean ± SEM; n = 6–9).

424

425 **Fig. 4. TUS-007 suppresses the growth of KRAS G12D-positive orthotopic**

426 **pancreatic tumors.**

427 **a,** Images showing the luciferase activity and total flux in orthotopic tumors

428 transplanted SW1990-Luc cells *in vivo*. **b,** Tumor growth (bioluminescence) in identical

429 mice treated with vehicle or TUS-007 administered p.o. every 3 days. (mean ± SEM; n

430 = 6). *P < 0.05 vs. vehicle alone. **c,** Representative histochemical staining of KRAS and

431 TUNEL in orthotopic tumor sections from the same mice used in **a**. The scale bar is 60

432 μm. **d,** Immunoblotting of KRAS G12D in tumor lysates from the same mice used in **a**.

433 The bar graph shows quantification of KRAS G12D normalized to GAPDH (mean ±

434 SEM; n = 6). **P < 0.01 vs. vehicle alone.

435

436 **Supplementary Fig. 1. Estimation of T_m value of KRAS G12D incubated with TUS-**

437 **007.**

438 KRAS G12D was mixed with DMSO, RAS-SOS inhibitor (4 μM) or TUS-007 (4 μM)

439 and incubated under heating from 25 °C to 99 °C. The denature of KRAS G12D was

440 monitored by the fluorescence. The typical curve of each group was shown in upper

441 panels. The means of T_m values were shown in lower table (mean ± SEM; n = 2). *P <

442 0.05 vs. DMSO, #P < 0.05 vs. RAS-SOS inhibitor.

443

444 **Supplementary Fig. 2. Effects of TUS-007 on proteasome activity levels.**

445 The levels of chymotrypsin-like (β5), trypsin-like (β2), and caspase-like (β1)

446 proteasome activities was monitored by Suc-LLVY-AMC, Bz-VGR-AMC, and Z-LLE-

447 AMC, respectively. AMC fluorescence was monitored by a plate reader with excitation

448 and emission filters of 360 and 460 nm, respectively (DMSO, 30 min = 1) (mean ±

449 SEM; n = 2–3).

450

451 **Supplementary Fig. 3. TUS-007 induced degradation of KRAS G12D/V in cell free**

452 **assay.**

453 **a,** The correlation between relative amount of KRAS G12D and concentration of TUS-

454 007 were approximated with Rodbard using the means of 3 independent examinations.

455 The DC50 was estimated about 4 μM**. b,** Successful KRAS G12V degradation by TUS-

456 007. KRAS G12V protein was incubated with TUS-007 at the indicated concentrations

457 in the presence of 26S proteasome for 1 h (mean ± SEM; n = 3). *P < 0.05 vs. DMSO.

458

459 **Supplementary Fig. 4. TUS-007 induced-degradation is proteasomal but**

460 **independent of ubiquitination in cells.**

461 GFP fused KRAS G12D and DsRed were transiently expressed in HeLa cells. The cells

462 were treated with TUS-007 in the presence of a proteasome inhibitor (MLN2238: upper

463 right), a ubiquitination inhibitor (NAEi: lower left) and a molecular chaperon inhibitor

464 (HSP70 inhibitor: VER-155008: lower right) for 24 h, and the ratios of GFP/DsRed

465 were measured by FACS.

466

467 **Supplementary Fig. 5. Selective chemical knockdown of RAS variants in RAS-less**

468 **MEFs expressing different types of human RAS.**

469 **a,** Relative viability of RAS-less MEFs expressing WT human RAS family members

470 after incubation with TUS-007 or DMSO. (mean ± SEM; n = 3–5). *P < 0.05 and **P <

471 0.01 vs. DMSO. **b,** Degradation of WT human RAS family members in RAS-less MEFs

472 treated with TUS-007 or DMSO for 72 h (mean ± SEM; n = 4–5). *P < 0.05 and **P <

473 0.01 vs. DMSO.

474

475 **Supplementary Fig. 6. FACS plots for Annexin V- PI staining of SW620-Luc cells.**

476 SW620-Luc cells were treated with the indicated agents for 48 h, followed by staining

477 with Annexin V-FITC and PI. The typical plots are shown.

478

479 **Supplementary Fig. 7. FACS plots for Annexin V- PI staining of HT-29-Luc cells.**

480 HT-29-Luc cells were treated with the indicated agents for 48 h, followed by staining

481 with Annexin V-FITC and PI. The typical plots are shown.

482

483 **Supplementary Fig. 8. TUS-007 induced apoptosis only when KRAS degradation**

484 **was detected in KRAS G12V driven cancer cells.**

485 SW620-Luc cells were treated with TUS-007 for 12 h (mean ± SEM; n = 3). The left

486 axis indicates KRAS/GAPDH, and the right axis indicates relative ratio of apoptotic

487 cells. *P < 0.05 vs. DMSO. The ratio of KRAS/GAPDH was determined by image

488 analyses of immunoblotting and ration of apoptotic cells were measured using FACS.

489

490 **Supplementary Fig. 9. Effects of TUS-007 on the growth of colon cancer**

491 **subcutaneous xenografts and toxicity.**

492 **a,** Comparison of SW620-Luc tumor weight at 21 days after injection (mean ± SEM; n

493 = 6–8). *P < 0.05 vs. vehicle alone. **b,** Immunoblotting of KRAS G12V chemical

494 knockdown in tumors from the same mice used in Fig. 2e (mean ± SEM; n = 6). **P <

495 0.01 vs. vehicle alone. **c,** Body weight changes in mice with SW620-Luc cells

496 transplanted subcutaneously (mean ± SEM; n = 6–8).

497

498 **Supplementary Fig. 10. TUS-007 induced apoptosis only when KRAS degradation**

499 **was detected in KRAS G12D driven cancer cells.**

500 SW1990 cell were treated with TUS-007 for 12 h (mean ± SEM; n = 3). The left axis

501 indicates KRAS/GAPDH, and the right axis indicates relative ratio of apoptotic cells.

502 *P < 0.05 vs. DMSO. The ratio of KRAS/GAPDH was determined by image analyses

503 of immunoblotting and ration of apoptotic cells were measured using FACS.

504

505 **Supplementary Fig. 11. Effects of TUS-007 on the growth of pancreatic cancer**

506 **subcutaneous xenografts and toxicity.**

507 **a,** Tumors of SW1990 cells from the same mice shown and comparison of tumor weight

508 in Fig. 3e at 21 days after p.o. administration (mean ± SEM; n = 6–9). *P < 0.05 vs.

509 vehicle alone. **b,** Tumor volume in mice with SW1990 cells transplanted

510 subcutaneously and treated with i.p. administered TUS-007 or vehicle (mean ± SEM; n

511 = 6–9). The agents were administered every three days. *P < 0.05 vs. vehicle. **c,** Body

512 weight changes in mice with SW1990 cells transplanted subcutaneously (mean ± SEM;

513 n = 6–9).

514

515 **Supplementary Fig. 12. Effects of oral treatment with TUS-007 on wild type RAS**

516 **in pancreas.**

517 The immunoblotting analyses of wt RAS proteins in pancreas from the same mice

518 shown in Fig. 3e (mean ± SEM; n = 6–9). *P < 0.05 vs. vehicle alone.

519

520 **Supplementary Fig. 13. Effect of TUS-007 on RAS signaling in pancreatic cancer**

521 **subcutaneous xenografts.**

522 Immunoblotting of KRAS and downstream signaling molecules in tumors from the

523 same mice used in Fig. 3e (**a**: p.o. treatment) and Supplementary Fig. 11c (**b**: i.p.

524 treatment). The quantitative analysis of the immunoblotting was shown as bar graph,

525 where the KRAS values were normalized to GAPDH, the p-ERK values were

526 normalized to the total ERK, and the p-AKT values were normalized to the total AKT

527 (mean ± SEM; n = 6). *P < 0.05 vs. vehicle.

528

529 **Supplementary Fig. 14. Effect of TUS-007 on growth of orthotopic pancreatic**

530 **cancer xenografts expressing mutant KRAS.**

531 **a,** Tumor growth, as assessed by luciferase signal, in individual mice orthotopically

532 transplanted SW1990-Luc cells treated with TUS-007 (orange) or vehicle alone (blue)

533 (mean ± SEM; n = 6). **b,** Pancreases from orthotopic xenograft model mice at day 21

534 after treatment with TUS-007 (lower-left panel) or the vehicle alone (upper-left panel)

535 and comparison of their weights (right graph) (mean ± SEM; n = 6). *P < 0.05 vs.

536 vehicle alone. **c,** The quantitative analyses of the KRAS G12D-positive area (left) and

537 TUNEL-positive area (right) in Fig. 4c (mean ± SEM; n = 6). **P < 0.01 vs. vehicle

538 alone. **d,** Body weight changes in mice subjected to orthotopic transplantation of

539 SW1990-Luc cells (mean ± SEM; n = 6).

540

541 **Supplementary Fig. 15. CANDDY induced degradation of MDM2, a common**

542 **undruggable target.**

543 **a,** The structure of MDM2-CANDDY using P53-MDM2 PPI inhibitor, with IC50 value

544 between 6-25 μM. **b,** MDM2-CANDDY degraded MDM2 in the dose dependent

545 manner. The human colon cancer cells HCT-116 were incubated for 48 h with MDM2-

546 CANDDY (mean ± SEM; n = 3). **P < 0.01 vs. DMSO.

547

548 **Supplementary Table 1. The concentration of TUS-007 in pancreas was**

549 **maintained for 72 h.**

550 The concentration of TUS-007 in pancreas from healthy wild-type mice i.p. treated with

551 TUS-007 at 80 mg/kg (means ± SEM; n = 5). The samples were obtained at indicated

552 time points after i.p. injection. The concentration of TUS-007 was measured with

553 HPLC.

554

555

556 **Methods**

557

558 **Cell lines.** SW1990 and HCT-116 cells were purchased from the American Type

559 Culture Collection (Manassas, VA, USA). SW620-Luc and HT29-Luc cells were

560 purchased from the National Institute of Biomedical Innovation, Health, and Nutrition

561 (Osaka, Japan). RAS-less MEF cell lines (wild-type (wt) KRAS, KRAS G12D, KRAS

562 G12V, KRAS G12C, NRAS and HRAS) were obtained from the National Institutes of

563 Health (NCI RAS Initiative at the Frederick National Laboratory for Cancer Research,

564 Frederick, MD, USA).

565

566 **Animal studies.** BALB/cA-nu/nu and BALB/cA (female, 7-9 weeks old) were

567 purchased from CLEA Japan (Tokyo, Japan). The animals were maintained in

568 conventional housing conditions, with a daily 12-h light/dark cycle, and given food and

569 water *ad libitum*. The animals were cared for in accordance with the NIH Guide for the

570 Care and Use of Laboratory Animals. All animal experiments were approved by the

571 Committee on Animal Experimentation of the Tokyo University of Science.

572

573 **Reagents.** MLN2238 (A10600) was purchased from AdooQ BioScience (Irvine, CA,
574 USA). NAEi was purchased from AdipoGen (San Diego, CA, USA). Human 26S
575 Proteasome Protein (E-365) and Human 20S Proteasome Protein (E-360) were
576 purchased from R&D Systems (Minneapolis, MN, USA). Human KRAS (G12D) and
577 the corresponding His tag (12259-H07E1) were purchased from Sino Biological
578 (Beijing, China). Human KRAS (G12V), 2-186, and the corresponding His tag (R06-
579 32BH) were obtained from SignalChem Lifesciences (Richmond, British Columbia,
580 Canada).
581
582 **Measurement of 20S proteasome activity.** The chymotrypsin-like (β5), trypsin-like
583 (β2), and caspase-like (β1) activities of the 20S proteasome were measured using a 20S
584 Proteasome Activity Kit GOLD (StressMarq Bioscience Inc., Victoria, British
585 Columbia, Canada). Purified 20S proteasome (0.1 μg) was incubated in the presence of
586 CANDDY molecules (1, 4, 10, 20, 40, 80, and 160 μM) or MLN2238 at the indicated
587 concentrations for 30 min at room temperature. After incubation, 100 mM of
588 fluorogenic peptide substrates, Suc-LLVY-AMC (β5 substrate), Bz-VGR-AMC (β2

589 substrate), or Z-LLE-AMC (β1 substrate), was added, followed by incubation for 1 h at

590 room temperature. The reaction mixture was then transferred to a 96-well plate, and the

591 fluorecence from hydrolyzed AMC groups was measured using a Synergy HT multi-

592 channel microplate reader (BioTek Instruments, Inc., Winooski, VT, USA) with a 360

593 nm excitation filter and 460 nm emission filter.

594

595 **Evaluation of affinity of TUS-007 for KRAS in a thermal shift assay.** The KRAS

596 G12D/V (100 nM) was preincubated with TUS-007, a RAS-SOS inhibitor, or 10%

597 DMSO in 75 mM phosphate buffer (pH 7.5) for 30 min at 37 °C (G12D) or for 20 min

598 at 25 °C (G12V). Aliquots of the reaction solution were sampled into separate

599 microtubes and heated for 30 min at 70, 80, or 90 °C for G12D, or at 40, 50, or 60 °C

600 for G12V. After centrifugation at 18,000 ×*g* for 20 min, the supernatants were analyzed

601 by SDS-PAGE, followed by immunoblotting using an anti-KRAS antibody (1:1000,

602 WH0003845MI, Sigma-Aldrich, St. Louis, MO, USA). Immunoreactive bands were

603 detected using an iBright CL1000 chemiluminator (Thermo Fisher Scientific, Waltham,

604 MA, USA) with an enhanced chemiluminescent substrate for detection of horseradish

605 peroxidase (HRP; Merck, Darmstadt, Germany).

606

607 **Estimation of T_m values using fluorescence based thermal shift assay.** To estimate

608 the T_m values, we performed a fluorescence based thermal shift assay using ProteoStat

609 Thermal Shift Stability assay (ENZO Life Sciences, Farmingdale, NY, USA). 1 μg of

610 KRAS G12D was mixed with DMSO (2.5 %), RAS-SOS inhibitor (4 μM) or TUS-007

611 (4 μM) in 1x assay buffer containing a fluorescent indicator of protein destabilization,

612 ProteoStat TS Detection Reagent, and incubated under heating from 25 °C to 99 °C in

613 StepOne Plus Real-time PCR system (Thermo Fisher Scientific). The kinetics of

614 fluorescent signals were analyzed to calculate T_m values in Protein Thermal Shift

615 Software 1.3 (Thermo Fisher Scientific).

616

617 **Evaluation of KRAS degradation induced by TUS-007 in a cell-free system.** KRAS

618 G12D (final concentration: 5 ng/μL) and 26S proteasome (final concentration: 8 nM)

619 were incubated with TUS-007 (2, 3, 5, 10, 20, 40 μM), RAS-SOS inhibitor (40 μM),

620 RAS-SOS-NH_2 (40 μM) or DMSO in 20 mM Tris-HCl buffer (pH 7.5) containing 20%

621 glycerol for 3 h at 37 °C. To assess the effect of MLN on chemical knockdown, KRAS

622 G12D and 26S proteasome were incubated with DMSO or TUS-007 40 μM in the

623 presence or absence of MLN (1 μM) in the same condition. KRAS G12V (final

624 concentration: 5 ng/μL) and 26S proteasome (final concentration: 8 nM) were incubated

625 with TUS-007 at the indicated concentration or DMSO in 75 mM phosphate buffer,

626 containing 1% LABRASOL (Gattefossé, Saint-Priest, France), for 1 h at 37 °C. After

627 centrifugation at 14,000 ×*g* for 10 min, the supernatants were analyzed by SDS-PAGE,

628 followed by immunoblotting using an anti-KRAS antibody (1:1000, WH0003845MI for

629 G12D, Sigma-Aldrich; and 1:2000, F234 for G12V, Santa Cruz Biotechnology, Inc.,

630 Dallas, TX, USA). The immunoreactive bands were detected, as described above. The

631 DC_{50} values were calculated by a Rodbard approximation using the band intensity

632 obtained from four and three independent experiments for G12D. Immunoblotting was

633 performed as mentioned above.

634

635 **Evaluation of target degradation in HeLa cells by flow cytometry.** The expression
636 plasmid pMIR-DsRed-IRES-ecDHFR-HA-GFP was a kind gift from Dr. L. Hedstrom
637 (Brandeis University). Plasmid expressing human KRAS G12D was constructed by RF
638 cloning with some minor modifications. A full-length cDNA clone of human KRAS
639 (AK292510) was obtained from the National Institute of Technology and Evaluation
640 (Tokyo, Japan). Hybrid RF cloning primers were designed using RF-Cloning.org. All
641 PCR amplifications were performed with KOD-Plus-Neo (Toyobo Co. Ltd., Japan). The
642 plasmid DNA sequences encoding target proteins were determined using an ABI 3500
643 (Applied Biosystems, MA, USA). HA-GFP-fusion target protein- and DsRed-
644 expressing HeLa cells were treated with 1% DMSO or CANDDY molecules in serum-
645 free medium for 24 h. The cells were harvested using trypsin and resuspended in
646 fluorescence activated cell sorter (FACS) buffer. The cells were then analysed on a BD
647 FACSCanto II. Data were analysed using FlowJo software (FlowJo LLC).
648
649 **Cell proliferation assay.** To examine the effect of TUS-007 on cell proliferation, the
650 WST-8 assay (Cell Count Reagent SF; Nacalai Tesque, Kyoto, Japan) was performed.

651 RAS-less MEF cells, expressing human RAS, were plated in 96-well plates at a density

652 of 3×10^3 cells per well, cultured overnight, then treated with the indicated

653 concentrations of TUS-007 in 4% FBS containing medium (KRAS G12D), 10% FBS

654 containing medium (KRAS G12V) or serum-free medium (KRAS G12C, wt KRAS,

655 HRAS, NRAS) for 72 h. After incubation, cell viability was measured

656 spectrophotometrically using the WST-8 reagent. The culture medium was removed and

657 WST-8 reagent was mixed with the growth medium at a ratio of 1:10 (with a final

658 volume of 110 μL) and added to each well. The cells were incubated in an atmosphere

659 of 5% CO_2 at 37 °C for 1 to 2 h, and the absorbance at 450 nm was measured using the

660 aforementioned Synergy HT multi-channel microplate reader (BioTek Instruments,

661 Inc.).

662

663 **Evaluation of TUS-007 specificity in cells.** RAS-less MEFs were used to evaluate the

664 selective degradation by TUS-007. RAS-less MEFs expressing one of the human WT

665 RAS members (KRAS WT, HRAS WT, or NRAS WT) or KRAS G12C were plated

666 into 6-well plates at a density of 3×10^4 cells per well, cultured overnight, and treated

667 with the indicated concentrations of TUS-007 in serum-free medium for 72 h. RAS-less

668 MEFs expressing KRAS G12D or G12V were plated into 96-well plates at a density of

669 3×10^3 cells per well, cultured overnight, and treated with the indicated concentrations

670 of TUS-007 in 4% FBS or 10% FBS containing medium, respectively, for 72 h. The

671 cells were lysed using RIPA buffer (Nacalai Tesque., Kyoto, Japan). The lysates were

672 centrifuged at 18,000 ×*g* for 10 min. The supernatants were analyzed by western

673 blotting using mouse monoclonal antibodies specific to KRAS (1:1000,

674 WH0003845MI; Sigma-Aldrich) and glyceraldehyde 3-phosphate dehydrogenase

675 (GAPDH, 1:10000, sc-32233; Santa Cruz Biotechnology, Inc.) and rabbit polyclonal

676 antibodies specific for HRAS (1:1000, 18295-1-AP; Proteintech, Rosemont, IL, USA)

677 and NRAS (1:1000, 10724-1-AP, Proteintech). Immunoreactive bands were detected

678 using iBright CL1000 chemiluminator or LAS 3000 (Fujifilm, Tokyo, Japan) with an

679 enhanced chemiluminescent substrate for the detection of horseradish peroxidase (HRP;

680 Merck, Darmstadt, Germany). The intensity of the RAS band was quantified using

681 ImageJ software and normalized to the intensity of the GAPDH band.

682

683 **Measurement of KRAS protein levels in cells by western blotting.** SW620-Luc and
684 SW1990 cells were treated with 1% DMSO or TUS-007 in serum-free medium for 12
685 or 48 h (SW620-Luc cells) and 12 or 72 h (SW1990 cells). The cells were lysed using a
686 RIPA buffer (Nacalai Tesque., Kyoto, Japan). The precipitates were separated from the
687 soluble fraction by centrifugation at 18,000 ×*g* for 20 min. The supernatants were
688 analyzed by western blotting with mouse monoclonal antibodies specific for KRAS
689 (1:1000, WH0003845MI; Sigma-Aldrich) and GAPDH (1:20000, sc-32233; Santa Cruz
690 Biotechnology, Inc.). The immunoreactive bands were detected by LAS-3000, as
691 described above. The intensity of the KRAS band was quantified using ImageJ software
692 and normalized to the intensity of the GAPDH band.
693
694 **Evaluation of caspase activity.** To measure caspase activity, SW1990 cells were plated
695 onto 96-well white plates and 96-well clear plates, at a concentration of 8×10^3
696 cells/well, in a medium containing 10% FBS. The plates were incubated overnight
697 without CO_2 equilibration at 37 °C. The medium was replaced with medium containing
698 2% FBS, DMSO, 100 μM TUS-007, 3 μM MLN2238, or 2.5 μM NAEi and incubated

699 for 96 h. SW620-Luc cells were plated onto 96-well white plates and 96-well clear

700 plates at 2×10^3 cells/well in medium containing 10% FBS. After overnight incubation,

701 the medium was replaced with FBS-free medium containing 1% L-glutamine, DMSO,

702 and 25, 100, or 500 μM TUS-007 for 48 h. The caspase 3/7 Glo assay (Promega,

703 Madison, WI, USA) was performed on the white plates according to the manufacturer's

704 protocol. The chemiluminescence intensity was measured with a Synergy HT plate

705 reader (BioTek). The cell viability was measured in the clear plates using the WST-8

706 assay, as described above. Caspase 3/7 activity was obtained as the chemical

707 luminescence intensity of the caspase 3/7 Glo assay normalized to the cell viability.

708

709 **Analysis of apoptosis by flow cytometry.** SW1990, SW620-Luc, and HT-29 cells

710 were seeded in 24-well plates, followed by the addition of compounds at the indicated

711 concentrations. After incubation for 12 or 48 h (SW620-Luc, HT-29) and 12 or 72 h

712 (SW1990), the cells were harvested using trypsin, washed with phosphate-buffered

713 saline (PBS), and pelleted by centrifugation at 110 $\times g$ for 5 min. The cells were

714 resuspended in 85 μL of binding buffer (Annexin V-FITC Kit, Medical & Biological

715 Laboratories Co., Ltd., Nagoya, Japan). Subsequently, 10 μL of annexin V-FITC and 5

716 μL of propidium iodide (PI) were added to each sample, followed by incubation in the

717 dark at room temperature for 15 min. After incubation, 400 μL of binding buffer was

718 added to each sample on ice. The cells were then analyzed using a FACSCanto II

719 fluorescence-activated cell sorter (BD Biosciences, Santa Clara, CA, USA) to detect the

720 fluorescein isothiocyanate (FITC) signal with excitation and emission filter wavelengths

721 of 488 nm and 580 nm, respectively, to detect the PI signal. Data were analyzed using

722 FlowJo software (FlowJo, Eugene, OR, USA).

723

724 **Subcutaneous xenograft model.** SW620-Luc (3×10^7 cells/mL) and SW1990 (5×10^7

725 cells/mL) cells were suspended in PBS, and 100 μL of the single-cell suspension was

726 transplanted subcutaneously into the right flanks of BALB/cA-nu/nu mice using a 26 G

727 syringe. Tumor volumes were calculated as the tumor length × width^2 × 0.5. When the

728 tumor volumes reached approximately 100 mm^3, the mice were randomized into

729 treatment and control groups of 6 to 8 animals per group. For i.p. treatment, TUS-007

730 was dissolved in DMSO and then diluted to a final concentration of 10% DMSO in 20%

731 polyethylene glycol (PEG) 400/Tween 80 (1:1 ratio). The TUS-007 solution was

732 administered intraperitoneally into the tumor-bearing mice at a dose of 80 mg/kg every

733 three days. The control mice were treated with the PEG/Tween vehicle alone. For p.o.

734 treatment, TUS-007 was suspended in 0.5% (w/v) carboxymethyl cellulose (CMC) and

735 administered p.o. at a dose of 80 mg/kg every three days. CMC (0.5% w/v) was

736 administered to control mice. Cetuximab was administered to an additional group of

737 SW620-Luc-implanted mice at a dose of 1 mg/mouse every three days.

738

739 **Orthotopic xenograft model.** The pGL4.51 (Luc2/CMV/Neo) vector (Promega) was

740 transfected into SW1990 cells. Successfully transfected cells were selected using G418.

741 SW1990-Luc cells were mixed with growth factor-reduced Matrigel (BD Biosciences)

742 on ice, at a ratio of 1:1 (v/v), to obtain a final cell density of 1.5×10^4 cells/μL. Ten

743 microliters of the cell suspension was injected directly into the pancreas of BALB/cA-

744 nu/nu mice using a 27 G syringe. Three days after cell transplantation, TUS-007

745 treatment was initiated in six mice. TUS-007 was suspended in 0.5% (w/v) CMC and

746 administered orally at a dose of 160 mg/kg every 3 days. CMC (0.5% w/v) was

747 administered to control mice (n = 6). Tumor luciferase activity was monitored based on

748 the bioluminescence intensity. Fifty microliters of D-luciferin (30 mg/mL in saline) was

749 injected subcutaneously in mice (Promega). Twenty minutes after the injection,

750 bioluminescence images were obtained using an IVIS Lumina LT (Perkin Elmer,

751 Waltham, MA, USA) with an exposure time of 15 s while the mice were under

752 isoflurane anesthesia (Wako, Tokyo, Japan).

753

754 **Measurement of RAS levels and downstream signaling molecule activation in**

755 **xenograft tumors.** KRAS expression in xenograft tumors and wt RAS protein

756 expression in pancreas were evaluated by immunohistochemistry and western blot

757 analysis. Tumor tissue and pancreas were harvested from the mice harboring

758 subcutaneous xenografts on day 21 of the TUS-007 administration. Tumor tissues were

759 harvested from the orthotopic xenograft mice on day 24 after the TUS-007

760 administration for consecutive 3 days starting on day 21. A portion of each sample was

761 fixed in 4% paraformaldehyde (Nacalai Tesque., Kyoto, Japan), embedded in paraffin,

762 then cut into 5 μm-thick sections. The sections were deparaffinized and incubated in

763 0.3% hydrogen peroxide in methanol for 30 min, and antigen retrieval was performed

764 using a 10 mM citrate buffer (pH 6.0) at 121 °C for 20 min. Tumor tissues were

765 subsequently blocked with 1% bovine serum albumin (BSA) in PBS for 30 min and

766 stained with primary antibodies specific for human KRAS (1:200, 12063-1-AP;

767 Proteintech), diluted in 1% BSA, followed by HRP-labeled secondary antibodies

768 (1:600, ab6721; Abcam, Cambridge, UK) in 1% BSA for 30 min at room temperature.

769 The sections were counterstained with hematoxylin and visualized with

770 diaminobenzidine (1.02924.0001; Merck). Digital images were obtained at 40×

771 magnification using a model BZ-9000 microscope (Keyence, Osaka, Japan). The area of

772 KRAS staining was quantified using ImageJ software, and the perimeter-to-area ratio

773 (KRAS-positive area/section) was calculated for a total of 30 images of 6 tumor

774 sections from each group. The remaining part of each tumor sample was homogenized

775 in a cell-lysis buffer (50 mM triethanolamine, 50 mM KCl, 5 mM $MgCl_2$, 0.25 M

776 sucrose, 1 mM phenylmethylsulfonyl fluoride, proteinase inhibitors (Nacalai Tesque.,

777 Kyoto, Japan), 1 mM dithiothreitol, and ribonuclease inhibitor (0.2 unit/μl, TaKaRa

778 Bio., Shiga, Japan) for western blot analysis, as described above. Mouse monoclonal

779 antibodies specific for KRAS (1:1000, WH0003845MI; Sigma-Aldrich), HRAS

780 (1:1000, 18295-1-AP; Proteintech, Rosemont, IL, USA), NRAS (1:1000, 10724-1-AP,

781 Proteintech) and GAPDH (1:20000, sc-32233; Santa Cruz Biotechnology, Inc.) and

782 rabbit antibodies specific for p-Erk1/2 (phospho-p44/42 MAPK) (1:1000, #4370; Cell

783 Signaling Technology, Beverly, MA, USA), Erk1/2 (p44/42 MAPK) (1:1000, #4695;

784 Cell Signaling Technology), p-Akt (1:2000, #4060; Cell Signaling Technology), and

785 Akt (1:2000; #4691; Cell Signaling Technology) were used for the

786 immunohistochemical staining. The immunoreactive bands were detected by LAS-3000

787 as described above. Quantitative analysis of the western blots was performed using

788 ImageJ software, and the results were normalized to the GAPDH band intensity.

789

790 **Measurement of apoptosis in xenograft tumors.** DNA fragmentation in the tumor

791 tissues was evaluated by a TdT-mediated dUTP nick-end labeling (TUNEL) assay.

792 Paraffin-embedded tissue sections (5 μm thick) were deparaffinized. The TUNEL

793 reaction was performed using the DeadEnd Fluorometric TUNEL System (Promega),

794 according to the manufacturer's instructions. Fluorescence images were acquired using a

795 BZ-9000 fluorescence microscope (Keyence). TUNEL-positive cells were identified

796 and counted using ImageJ software. In total, 30 images of 6 tumor sections were

797 analyzed from each group.

798

799 **Determination of TUS-007 in pancreas.** BALB/cA mice were treated i.p. with TUS-

800 007, and pancreas tissue was collected at suitable time points. Approximately 30-60 mg

801 of tissue was homogenized in 0.6 mL of tissue-lysis buffer (50 mM Tris-HCl pH 8.0, 20

802 mM EDTA, 10 mM NaCl, 1% SDS) by Micro Smash MS-100 using stainless (5.5 ϕ) and

803 zirconia (1.0 ϕ) beads (TOMY SEIKO CO., LTD., Tokyo, Japan), and 1 μL propyl p-

804 hydroxybenzoate (4 mg/mL in DMSO) was added to each sample as an internal standard.

805 Lysates were centrifuged at 18,000 ×*g* for 10 min and 2.25 mL of methanol/chloroform

806 (ratio of 2:1) was added to the supernatants and the mixture was allowed to stand for 30

807 min at room temperature. Chloroform and distilled water (0.75 mL each) were added and

808 samples were centrifuged at 1,500 ×*g* for 15 min. The layer of chloroform was collected.

809 The supernatants were dried under reduced pressure and redissolved in the mobile phase.

810 TUS-007 was determined by HPLC (Alliance e2695, Waters Corporation., MA, USA)

811 using COSMOSIL® C18-AR-II column (150×4.6 mm, Nacalai Tesque., Kyoto, Japan) in

812 the isocratic elution mode with 0.1% trifluoroacetic acid (TFA) in 50:50 (v/v)

813 acetonitrile/water mobile phase at a flow rate of 1.0 mL/min. All reagents for the assay

814 were purchased from Nacalai Tesque. (Kyoto, Japan).

815

816 **Degradation of MDM2 in HCT-116 cells.** HCT-116 human colon-cancer cells were

817 treated with 1% DMSO or TUS-007 in serum-free medium for 24 h. The cells were

818 lysed using a RIPA buffer (Nacalai Tesque). The precipitates were separated from the

819 soluble fraction by centrifugation at 18,000 ×*g* for 20 min. The supernatants were

820 analyzed by western blotting using a rabbit polyclonal antibody specific for MDM2

821 (1:1000, sc-965, Santa Cruz Biotechnology, Inc.) and GAPDH (1:20000, sc-32233;

822 Santa Cruz Biotechnology, Inc.). The immunoreactive bands were detected by LAS-

823 3000, as described above. The intensity of the MDM2 band was quantified using

824 ImageJ software and normalized to the intensity of the GAPDH band.

825

826 **Statistical analyses.** Statistical significance was determined with JMP® Pro 14 (SAS

827 Institute Inc., Cary, NC, USA). An unpaired *t*-test was used to compare pairs of groups

828 under the assumption of normality. A one-way ANOVA with Dunnett's post hoc

829 analysis was used to compare sets of three or more groups. P-values < 0.05 were

830 considered statistically significant.

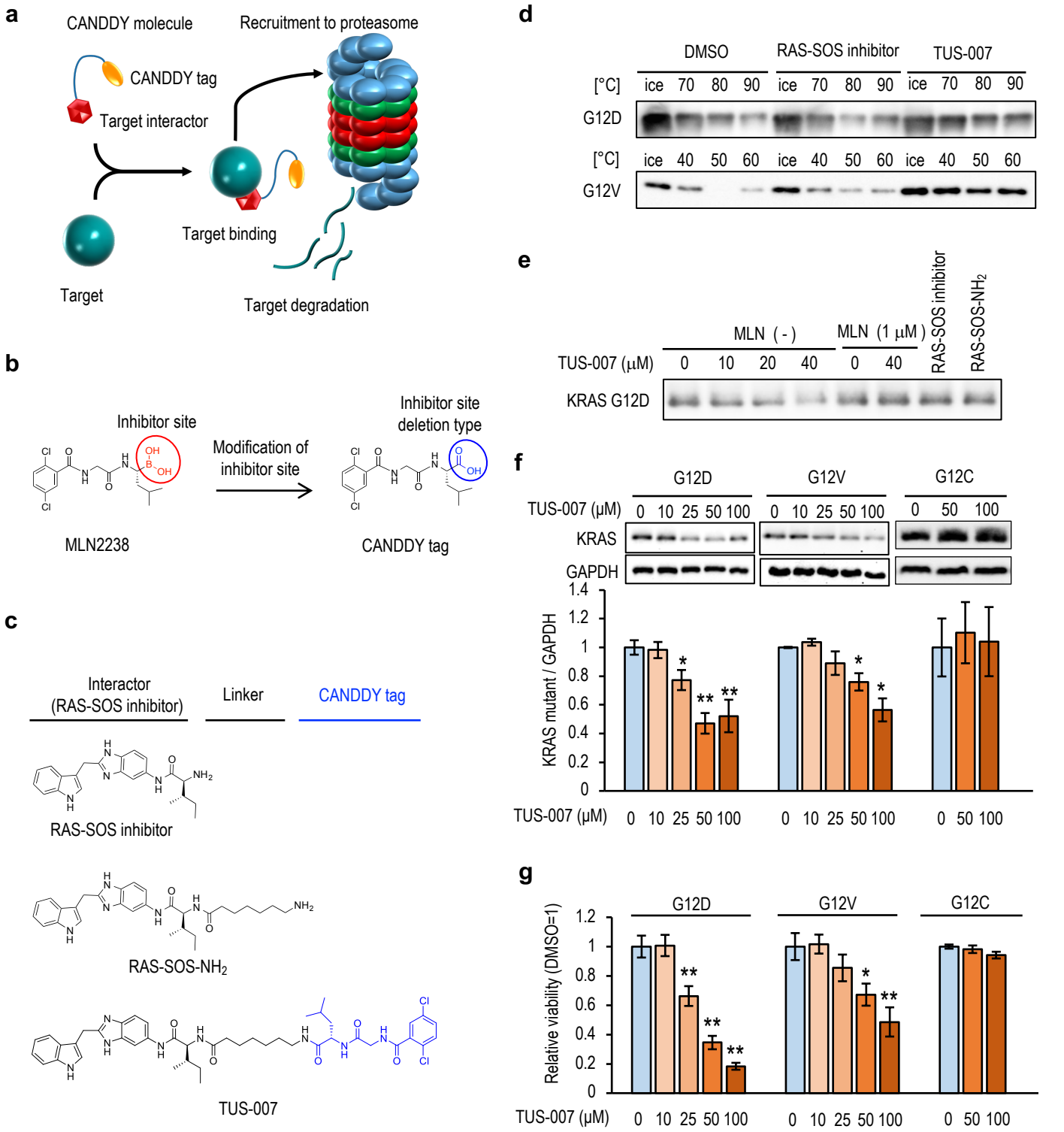

Fig. 1. RAS chemical knockdown *in vitro*.
a, Principle of the CANDDY technology. Each CANDDY molecule includes a target interactor (burgundy hexagon) and a CANDDY tag (yellow oval). The target protein is bound by the CANDDY molecule *via* the target interactor and is directly degraded by proteasome via the CANDDY tag. **b,** The CANDDY tag was synthesized by chemically inactivating the inhibitor site of MLM2238 (MLN). **c,** Structures of the RAS-SOS inhibitor (ref. 5), RAS-SOS-NH_2, and TUS-007. **d,** Evaluation of the target-binding affinity of TUS-007 to KRAS mutants by a thermal shift assay. Recombinant KRAS was treated with the vehicle, RAS-SOS inhibitor, or TUS-007 for 30 min, heated at the indicated temperature for 20 min, then analyzed by immunoblotting. **e,** TUS-007 induced KRAS G12D chemical knockdown by 26S proteasome in a cell free assay. KRAS G12D incubated with 26S proteasome and agents as indicated for 3 h. **f & g,** RAS-less MEFs expressing KRAS G12D, G12V or G12C were incubated with TUS-007 for 72 h. Representative blots of KRAS are shown (**f**). The relative amounts of KRAS mutants normalized to GAPDH are shown in the bar graph (mean ± SEM; n = 3–4). The cell viability was also measured (mean ± SEM; n = 3–4) (**g**). *P < 0.05 and ** P < 0.01 vs. DMSO.

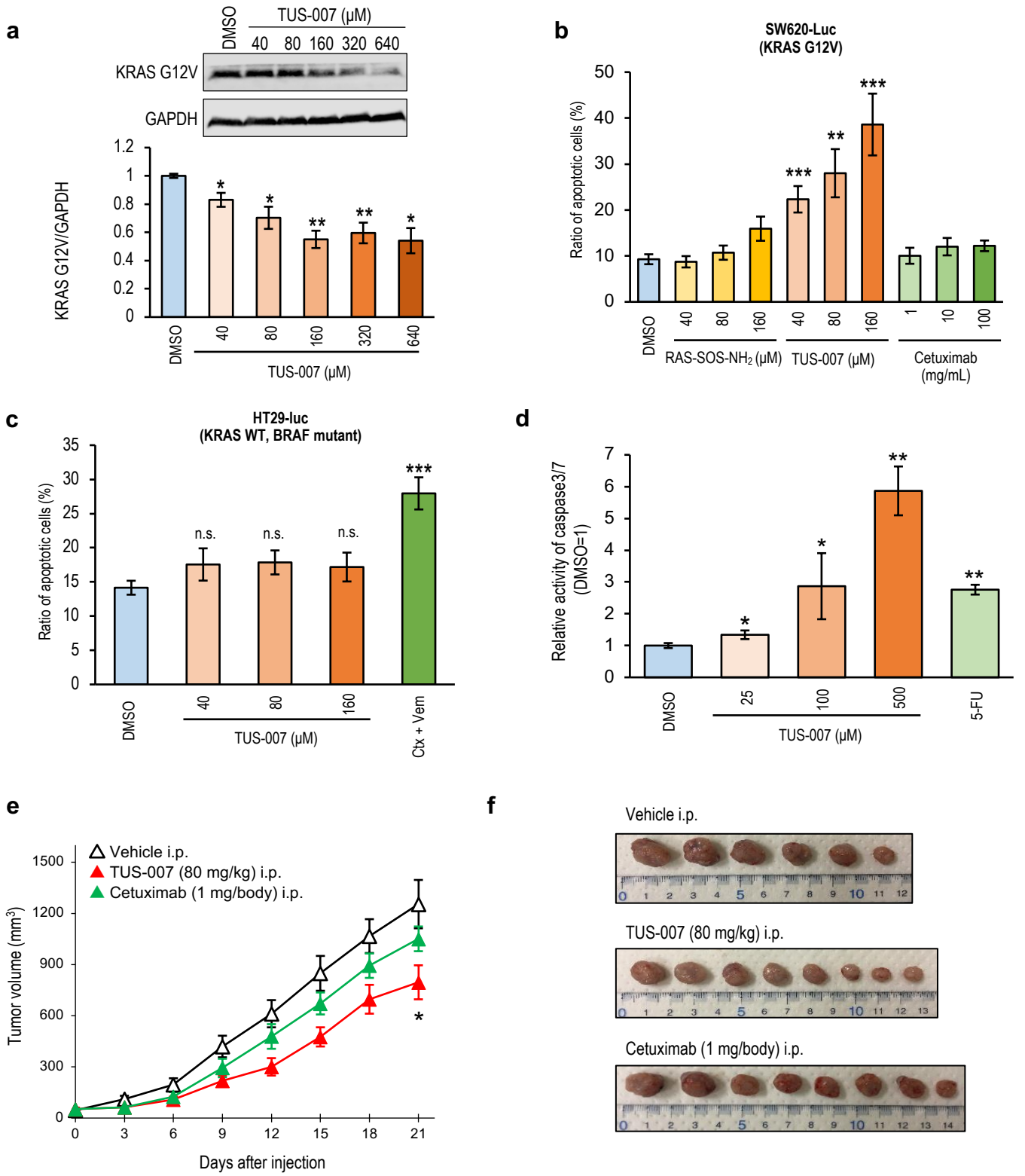

Fig. 2. Chemical knockdown and tumor suppression *in vitro* and *in vivo* in KRAS G12V-driven human colon cancer cells by TUS-007 treatment.

a, Immunoblotting analysis of KRAS G12V chemical knockdown in SW620-Luc cells treated with TUS-007 for 48 h at the indicated doses. The KRAS band intensity was normalized to that of GAPDH (mean ± SEM; n = 3). *P < 0.05 and **P < 0.01 vs. DMSO. **b & c,** The ratio of apoptotic cells were analyzed in colon cancer SW620-Luc cells (**b**) and HT29-Luc cells (**c**), a KRAS-independent, BRAF-dependent cell line (Ctx + Vem: 100 μg/ml cetuximab and 40 μM vemurafenib). Cells were treated with each compound for 48 h in terms of the number of annexin V-positive/PI-negative apoptotic cells detected by flow cytometry (mean ± SEM; n = 2–5). **P < 0.01, and ***P < 0.001 vs. DMSO. **d,** Relative activity of caspase 3/7 in SW620-Luc cells treated with TUS-007 or 5-fluorouracil (5-FU) for 48 h (mean ± SEM; n = 3). *P < 0.05 and **P < 0.01 vs. DMSO. **e,** Tumor volume in mice with SW620-Luc cells transplanted subcutaneously and treated with i.p. administration every 3 days (mean ± SEM; n = 6–8). *P < 0.05 vs. vehicle alone. **f,** Tumors of SW620-Luc cells at day 21 from the same mice shown in **e** (n = 6–8).

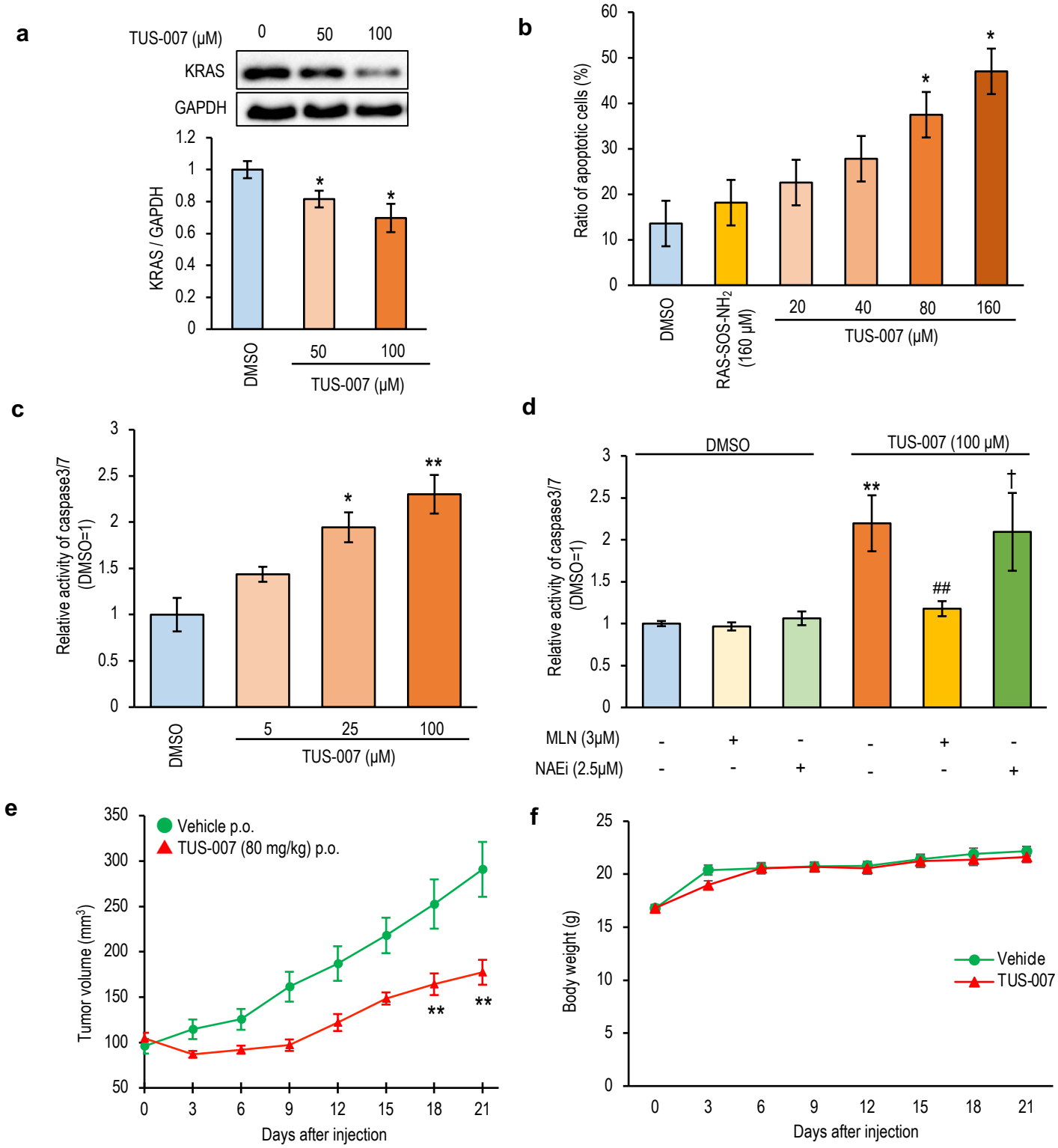

Fig. 3. Chemical-knockdown and tumor suppression *in vitro* and *in vivo* in KRAS G12D-driven human pancreatic cancer cells by TUS-007 treatment.

a, KRAS G12D chemical knockdown induced by TUS-007 in SW1990 cells. SW1990 cells were treated with TUS-007 for 72 h and analyzed by immunoblotting. The KRAS G12D band intensity was normalized to that of GAPDH (mean ± SEM; n = 4). *P < 0.05 vs. DMSO. **b,** The proportion of annexin V-positive apoptotic SW1990 cells treated with DMSO, RAS-SOS-NH_2 or TUS-007 for 72 h (mean ± SEM; n = 3). *P < 0.05 vs. DMSO or RAS-SOS-NH_2. **c,** TUS-007 increased the caspase 3/7 activity in SW1990 cells after treatment for 96 h (mean ± SEM; n = 3). *P < 0.05 and **P < 0.01 vs. DMSO. **d,** Caspase 3/7 activation by TUS-007 was proteasome dependent and ubiquitination independent. SW1990 cells were treated with the agents for 96 h (mean ± SEM; n = 3). **P < 0.01 vs. DMSO, ##P < 0.01 vs. TUS-007 (100 μM) only, and †no statistically significant difference compared with TUS-007 (100 μM) only. **e,** Tumor volume in mice with SW1990 cells transplanted subcutaneously and treated with p.o. administered TUS-007 or vehicle (mean ± SEM; n = 6–9). The agents were administered every 3 days. **P < 0.01 vs. vehicle alone. **f,** Body weight changes in mice with SW1990 cells transplanted subcutaneously (mean ± SEM; n = 6–9).

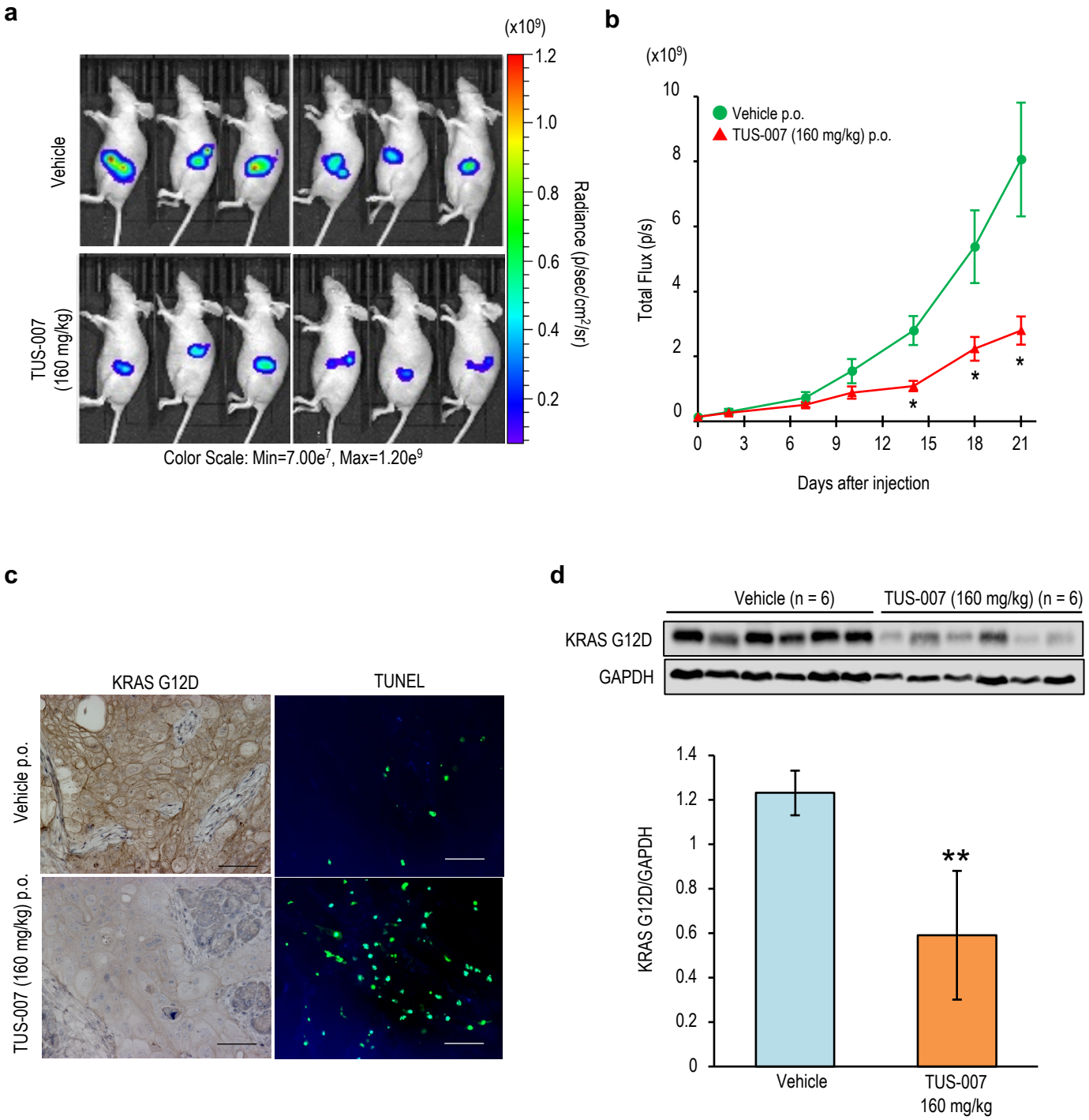

Fig. 4. TUS-007 suppresses the growth of KRAS G12D-positive orthotopic pancreatic tumors.
a, Images showing the luciferase activity and total flux in orthotopic tumors transplanted SW1990-Luc cells *in vivo*. **b,** Tumor growth (bioluminescence) in identical mice treated with vehicle or TUS-007 administered p.o. every 3 days. (mean ± SEM; n = 6). *P < 0.05 vs. vehicle alone. **c,** Representative histochemical staining of KRAS and TUNEL in orthotopic tumor sections from the same mice used in **a**. The scale bar is 60 μm. **d,** Immunoblotting of KRAS G12D in tumor lysates from the same mice used in **a**. The bar graph shows quantification of KRAS G12D normalized to GAPDH (mean ± SEM; n = 6). **P < 0.01 vs. vehicle alone.